IEEE Access
Multidisciplinary | Rapid Review | Open Access Journal

Received 28 January 2023, accepted 23 February 2023, date of publication 28 February 2023, date of current version 19 July 2023.

Digital Object Identifier 10.1109/ACCESS.2023.3250558

RESEARCH ARTICLE

An Improved Whale Optimization Algorithm Based PIDF–(1+PI) Cascade Automatic Generation Control for Multi-Area Multi-Source Power System With Capacitive Energy Storage

JINGFENG MAO[1], RUNDA LIU[1], AIHUA WU[1], SHANG WU[2], AND JIANJUN HE[2]
[1]School of Electrical Engineering, Nantong University, Nantong 226019, China
[2]Nantong Offshore Construction and Engineering Company Ltd., Nantong 226019, China

Corresponding author: Aihua Wu (wu.ah@ntu.edu.cn)

This work was supported in part by the Natural Science Research Program of Jiangsu Colleges and Universities under Grant 20KJA470002, and in part by the Excellent Teaching Team of ''Qinglan Project'' of Jiangsu Colleges and Universities.

ABSTRACT Modern power system has complex composition structure and high stability operation requirements. While the emergence of various new energy sources and the uncertainty of external disturbances bring a great challenge to the Automatic Generation Control (AGC) of power system. In order to improve the robustness of the AGC and facilitate the practical engineering application, this paper proposes a novel structure multistage Proportional Integral Derivative (PID) cascade automatic generation controller as well as an improved more effective control parameter optimization algorithm. Firstly, a two-area multi-unit multi-source hydro/thermal power system containing with capacitive energy storage unit is modeled. And using double closed-loops control method, a PID controller with derivative Filter and 1+Proportional Integral unit (PIDF-(1+PI)) cascade automatic generation controller is proposed. Secondly, by introducing a nonlinear time-varying adaptive weight factor, an improved Whale Optimization Algorithm (WOA-w) is proposed to accelerate the convergence speed and enhance the solution accuracy. Then, based on the integral of time multiplied absolute error (ITAE) objective function, the proposed PIDF-(1+PI) controller parameters are optimized by WOA-w. Finally, MATLAB/Simulink software is used to implement the control system multi-case simulation. Compared with other three control strategies, the multi-scenario cases simulation results verify the correctness and effectiveness of the proposed control strategy.

INDEX TERMS Automatic generation control, cascade control, hydro thermal system, whale optimization algorithm, capacitive energy storage.

NOMENCLATURE

α_{12}	Power coefficient
P_{r1}, P_{r2}	Capacity for area-1, area-2.
PF_T, PF_H	Participation factors of thermal and hydro units.
T_G	Speed governor time constant of the thermal unit.
T_T	Turbine time constant of the thermal unit.
K_R	Reset time of the hydraulic amplifier.
T_{RH}	Hydro governor time constant.
T_R	Hydro governor reset time.
T_{GH}	Hydro governor transient droop time constant..
T_W	Hydro turbine time constant..
K_P	Power system gain constant.
T_P	Power system time constant.
T_{12}	Tie-line synchronizing coefficient.
ΔF_i	Frequency deviation signal for area-i.
T_1, T_2, T_3, T_4	Time constants of two-stage phase compensation blocks.

The associate editor coordinating the review of this manuscript and approving it for publication was Siqi Bu.

K_{CES}	Gain of CES unit.
T_{CES}	Time constant of CES unit.
ACE_i	Area control error.
B_1, B_2	Frequency response characteristics of area-1 and area-2.
$(X_{best}, Y_{best}, Z_{best})$	Optimal position in 3D space.
D_b	Enclosing step length.
D	Step length.
D_d	Distance between the current individual whale and the current best whale individual.
b	Constant for defining the shape of the logarithmic spiral.
l,	Random number in [−1,1].
l,	Random number in [−1,1].
ω	Nonlinear time-varying adaptive weight.
V_no	Number of design variables.
$f_{\min}$	Optimal value of benchmark functions.
ΔP_{gi}	Area-i power generation.
ΔP_{Di}	Step load perturbation in area-i.
K_P	Proportional of PIDF controller.
K_I	Integral of PIDF controller.
K_D	Derivative of PIDF controller.
N	Derivative filter gains of PIDF controller.
K_{P1}	Proportional of 1+PI controller.
K_{I1}	Integral of 1+PI controller.
K_P^{min}	Minimum value of proportional of PIDF controller.
K_P^{max}	Maximum value of proportional of PIDF controller.
ΔP_{refi}	Controller output of area-i.
R_1, R_2	Speed governor regulation parameter.
p	Probability factor.
A and C	Coefficient vector.
r_1 and r_2	Random numbers in [0, 1].
a	Control parameter.
$Maxi$	Maximum number of iterations.
m	Number of iterations.
$X_R(m)$	Random position vector.
$X(m)$	Position vector.
(X, Y)	Individual position.
(X_{best}, Y_{best})	Optimal position in 2D space.
K_I^{min}	Minimum value of integral of PIDF controller.
K_I^{max}	Maximum value of integral of PIDF controller.
K_D^{min}	Minimum value of derivative of PIDF controller.
K_D^{max}	Maximum value of derivative of PIDF controller.
N^{min}	Minimum value of derivative filter gains of PIDF controller.
N^{max}	Maximum value of derivative filter gains of PIDF controller.
K_{P1}^{min}	Minimum value of proportional of PIDF controller.
K_{P1}^{max}	Maximum value of proportional of PIDF controller.
K_{I1}^{min}	Minimum value of integral of 1+PI controller.
K_{I1}^{max}	Maximum value of integral of 1+PI controller.
K	Population size.

I. INTRODUCTION

With the development of industry, the complexity of power systems is increasing. The access of large-scale new energy sources brings stronger perturbations to the power system. The main aspiration of the power system is to deliver stable power continuously to consumers. Ensuring the stability, safety and reliability of the power system are the key to supply a continuous, high-quality electric power. The stability of frequency is an important indicator of power quality. Automatic Generation Control (AGC) technology plays a vital role in maintaining the power balance, the frequency stability, and the power quality. The key objective of AGC is to control the generation frequency and exchange power of adjacent areas, as well as to enable the system frequency and area tie-line power stable at the rated values whether the system works normally or suffers from large load perturbations [1], [2], [3], [4]. In addition to the ability to suppress load perturbations, the AGC should have strong robustness to resist the uncertainty of system parameters and randomness of load change. Therefore, a strong robust and responsive AGC controller is needed for complex modern power system to obtain the desired work performance.

In the past decades, AGC strategies have been intensively studied in many literatures to improve the work performance of power system under normal or perturbed conditions. And, it can be seen that the proportional integral derivative (PID) controller is still the mainstream controller in the current research for AGC, and the structure of the controller and the selection of parameters play a decisive role in the performance of AGC to a large extent [2], [5].

To find the optimal controller parameters, modern metaheuristic algorithms are widely used for controller parameter selection. presents the optimal design and implementation of PI structured optimal AGC controller using full state vector feedback control theory for a 2-area power system model consisting of hydro, thermal, and gas power plants in the presence of WPPs. In [6], a Firefly Algorithm (FA) optimized PID controller is proposed to design the AGC for combined cycle gas turbine units. In [7], a Quasi-oppositional Gray Wolf Optimization (QOGWO) optimized PID controller is proposed to design the load frequency control (LFC) for large-scale power system. In [8], a Differential Evolution (DE) algorithm-optimized PID controller is proposed to solve the optimal parameter tuning of the AGC controller for the interconnected grid. However, the simplicity of the PID

controller makes it difficult to obtain the optimal performance of the system. This is because the design tradeoff between the integral and derivative gains of the PID controller usually makes it difficult to achieve optimal performance. For example, increasing the integration gain to reduce steady-state error can lead to undesired transient responses. Therefore, the integration term can only be automatically activated in the steady-state portion of the response to reduce or eliminate steady-state error [9]. Reference [10] presents the optimal design and implementation of PI structured optimal AGC controller using full state vector feedback control theory to overcome the disadvantages of the PI controller.

In addition, many references started to change the structure of the controller to overcome the disadvantages of the PID controller and to obtain the optimal performance of the system. Reference [11] proposes a fuzzy PID controller based on the Imperial Competition Algorithm (ICA), which combines the fuzzy controller with the PID controller and extends it to a two-area reheat thermal-PV grid system. Reference [12] proposes an ICA optimized new design of intelligent multi-stage fuzzy assisted PID with filter-(1+PI) (FPIDF-(1+PI)) controller and applies it to an AGC system with capacitive energy storage (CES). However, both [11] and [12] are optimized using the traditional ICA, which has the disadvantage of easily falling into the local optimum. Reference [5] proposes to use a hybrid Stochastic Fractal Search (SFS) and Local Unimodal Sampling (LUS) based multistage PID controller and extends to a three unequal area system power system with appropriate nonlinearities such as Generation Rate Constraint (GRC), Governor Dead Band (GDB) and time delay.

In addition to these, cascade controllers are widely used in AGC systems. Cascade controllers are more appropriate over traditional controllers to tracking the preset-point and resisting the perturbation. And as underscored by many researches, a definite cascaded control scheme has potential to offer better performance than the classical feedback controller [13]. Reference [14] proposes a PD-PID cascade controller based on the optimization of the Bat algorithm, and verifies the superiority of the series control strategy in AGC system. But the Bat algorithm has the disadvantages of slow convergence speed and low solution accuracy in the late work stage. Reference [15] proposes a Modified Grey Wolf Optimization (MGWO) optimized PI-PD cascade controller and applies it to the AGC of power system with Plug in Electric Vehicles (PEV). Meanwhile, the simple structure of the inner and outer loop controllers of the cascade controllers proposed in [14] and [15] make it difficult to obtain the best performance of the system. Reference [16] proposes a cascade PID-PID controller based on a new hybrid scheme of the improved Teaching Learning Based Optimization - Differential Evolution (hITLBO-DE) algorithm optimization, which is applied to the AGC of a power system with multiple renewable energy sources, with a large improvement in the optimization algorithm. Reference [17] applies the hITLBO-DE optimized cascade PID controller to 2-area multi-non-conventional system with communication time delay and energy storage, and verifies that the cascade controller maintains stable performance even in the presence of communication time delay. But the inner and outer loops of its cascade controller use PID control strategy, and the structure of the controller is relatively simple. Reference [18] proposes ICA optimized fuzzy fractional order (FO) PI-FOPID (FFOPI–FOPID) cascade controller, and validates its control performance in a single and interconnected multi-area thermal power system. However, the same as [11], [12], and [18] uses the traditional ICA algorithm for optimization, it has great potential for improvement. Reference [19] proposes a Marine Predator Algorithm (MPA) optimized proportional integral derivative acceleration - proportional integral derivative acceleration (PIDA-PIDA) cascade load frequency controller, but MPA is too complex and it has disadvantages such as slow convergence and low solution accuracy. Reference [20] proposes a Dragonfly Search Algorithm (DSA) optimized (1+PD)-PID cascade controller for diverse electric power system, and verifies the superior performance of the cascade controller. Reference [21] presents an extensive comparative analysis among different optimized controllers for frequency regulation, the results show that the performance of the cascade controllers are significantly better than that of the non-cascade controllers. Reference [22] proposes a novel parameter sensitivity-based GA (PSA) optimization algorithm to design the LFC. And the PSA optimized cascade PI-PD with filter (PI-PDN) controller performs better than the traditional PI-PDN controller, according to the test results of multi-scenario cases simulation and real-time hardware-in-the-loop experiment.

For the complex modern power system, it is very challenging to design a good AGC control strategy. The control strategy not only needs high robustness to deal with strong disturbances and uncertain operating conditions, but also needs to be easily implemented to adapt to practical engineering applications.

To improve the current AGC control strategy, the shortcomings of the current AGC strategy need to be addressed. The main disadvantages of the current control strategy exist mainly in the controller structure as well as in the optimization algorithm. The controller with a too simple structure often difficult to obtain the best performance of the system because there are too few controller parameters that can be adjusted. The complex controllers are suffering from complex control laws in addition to demanding several tunable design parameters, and often have problems such as more conservative stability margin and difficulty in implementation in actual engineering applications [20]. The current common traditional metaheuristic algorithm often has the disadvantages of low solution accuracy, low convergence accuracy, slow convergence speed, and easy falling into local optimum [23]. According to the actual situation of automatic power generation control, the optimization algorithm of the controller, not only needs to effectively optimize the controller parameters,

but also needs to complete the parameter optimization in a relatively short time [24].

For this reason, this paper designs the PIDF-(1+PI) cascade controller, which can better limit the influence of load perturbations on the system and improve the dynamic response performance of the system by using cascade control compared with the traditional PID controller. And inspired by [25] and [26], the traditional Whale Optimization Algorithm (WOA) [27] is improved by a nonlinear time-varying adaptive weight to obtain the WOA-w. The WOA originates from the simulation of the unique feeding behavior of humpback whales. WOA is conceptually simple, can be implemented quickly, and requires fewer parameters to be tuned. The WOA transitions between different phases of the algorithm by updating the optimal solution with probability values. These advantages allow WOA to quickly complete parameter optimization in the face of complex power system. Along with these advantages, traditional WOA has the disadvantages of slow convergence and the tendency to fall into local optimal solutions. To overcome these disadvantages, WOA-w is used to adjust the coefficient vector according to the change of the weight factor with the number of iterations to improve the exploration capability of the algorithm, avoid falling into a local optimum, and enhance the convergence speed.

In addition to improving control strategies, energy storage systems (ESS) have great potential for maintaining power balance and frequency stability during load perturbations to support AGC. Research has shown that flexible AC transmission systems (FACTS) based on ESS such as superconducting energy storage (SMES), redox liquid batteries (RFB), and capacitive energy storage (CES) are very effective in suppressing unexpected load perturbations by adding or absorbing the required power to the grid. ESS have a more significant positive effect on system frequency regulation in a shorter period than conventional network assets due to their fast response capability, and thus, satisfy the requirements of AGC [28], [29]. CES has received increasing theoretical and experimental attention due to its great potential in modern power system. The Spanish government-supported STORE project has installed CES systems of 4 MW/20 MW for frequency stabilization and control enhancement in the La Palma power system in Spain [30]. The 60MW pulsed power system based on CES for smoothing the power demand-supply of the magnets of a particle accelerator (CERN) is an example of its high-power application in power system [31]. For this purpose, a two-area multi-unit multi-source hydro/thermal power system [12], [32] with capacitive energy storage unit is selected as a power system model in this paper.

In summary, the main contributions of this paper include: (1) A novel structure PIDF-(1+PI) cascade controller is proposed for the multi-area multi-source hydro/thermal power system with capacitive energy storage devices. (2) The WOA-w is obtained by improving the traditional WOA through a nonlinear time-varying adaptive weight, and is used to optimize PIDF-(1+PI) cascade controller parameters. (3) The dynamic performance of the proposed cascade control strategy is compared with that of the cascade control strategies of FA-optimized PID, hSFS-LUS optimized PDF-(1+PI), and GWO optimized PIDF-(1+PI). (4) Multi-scenario case simulations are implemented, including different load perturbation forms, load perturbation areas range, system parameters changes and the nonlinearity effects, to verify the correctness and effectiveness of proposed cascade control strategy.

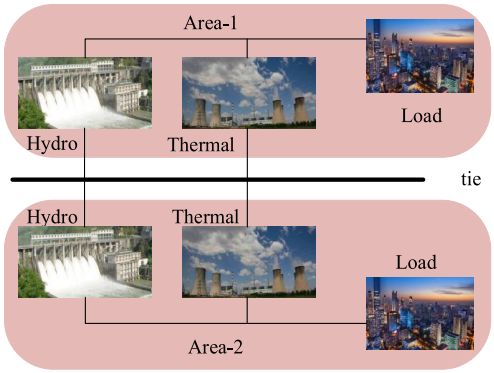

FIGURE 1. The two-area multi-unit multi-source hydro/thermal power system.

This paper consists of seven sections. The section I introduces the research topic. Section II introduces the power system model studied in this paper. Section III discusses the structure, concept and advantages of the proposed PIDF-(1+PI) controller. Section IV presents the improved WOA-w optimization algorithm, and algorithm analysis and selection of the objective function. Section V focuses on the multi-scenario case simulations, as well as discussion and analysis of the results. Section VI presents the robustness analysis of the proposed WOA-w optimized PIDF-(1+PI) cascade control strategy. Section VII concludes the whole paper.

II. SYSTEM MODELING

A. POWER SYSTEM MODEL

The two-area multi-unit multi-source hydro/thermal power system shown in Fig.1 has two control areas [12], [32]. Each area has hydro and thermal power plants respectively. Each area is subject to load perturbations. The two areas are connected via a tie-line for power transfer between areas to improve reliability and stability [32]. Based on the original system, a capacitive energy storage (CES) device is equipped in each area to optimize the automatic power generation control effect. The transfer function model of Fig. 1 is shown in Fig. 2. In the transfer function model, both the areas are 2000 MW and nominal load is 1000 MW, and the power coefficient is α_{12} given by

$$\alpha_{12} = -\frac{P_{r1}}{P_{r2}} \tag{1}$$

where, P_{r1}, P_{r2} are the capacity for area-1, area-2 respectively.

In the transfer function model, the thermal unit contains two modules of the governor and turbine; the hydro unit

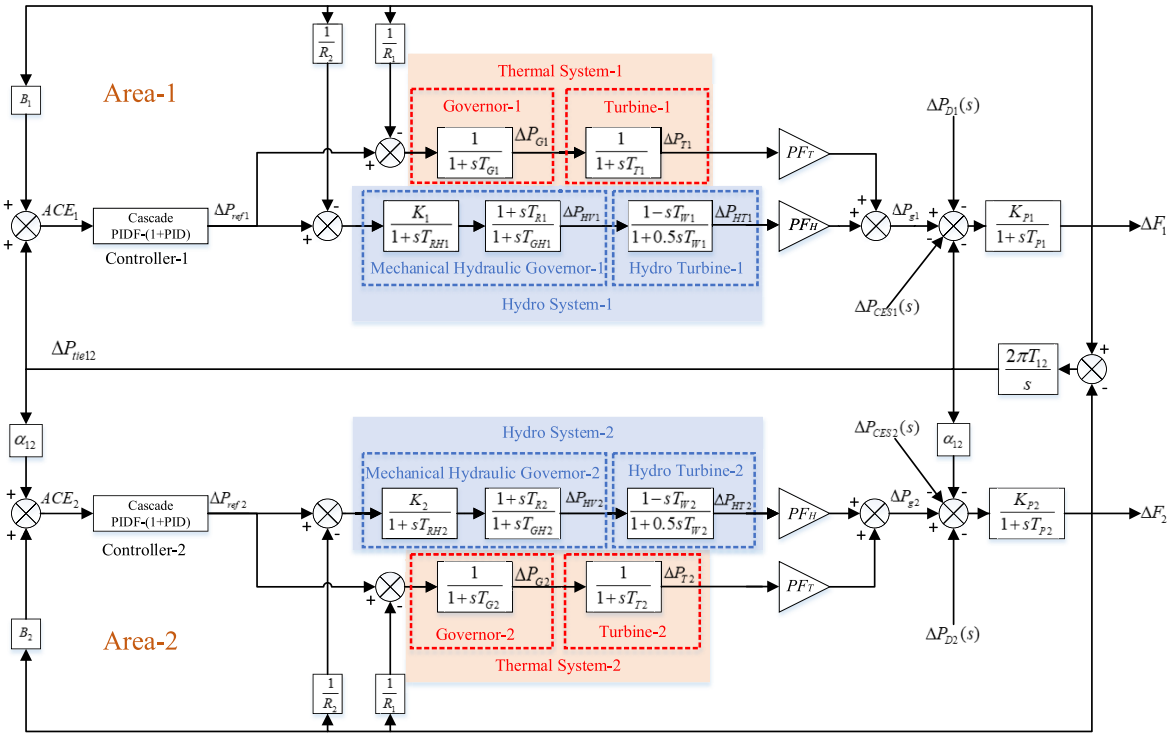

FIGURE 2. Transfer function model of two-area multi-unit multi-source hydro/thermal power system.

contains two modules of the mechanical hydraulic governor and turbine. Participation factors of thermal (PF_T) and hydro (PF_H)units are $PF_T = PF_H = 0.5$.

For the thermal unit, the speed governor is represented by the transfer function

$$G_G(s) = \frac{1}{1 + sT_G} \tag{2}$$

where, T_G is the speed governor time constant in the thermal unit.

The turbine is represented by the transfer function

$$G_T(s) = \frac{1}{1 + sT_T} \tag{3}$$

where, T_T is the turbine time constant in the thermal unit.

For the hydro unit, the mechanical hydraulic governor is represented by the transfer function

$$G_{GH}(s) = \left(\frac{K_R}{1 + sT_{RH}}\right)\left(\frac{1 + sT_R}{1 + sT_{GH}}\right) \tag{4}$$

where, K_R is the reset time of the hydraulic amplifier, T_{RH} is the hydro governor time constant, T_R is the hydro governor reset time, T_{GH} is the hydro governor transient droop time constant.

Hydro turbine used in hydro unit has different characteristics from thermal turbines, and it is represented by the transfer function

$$G_{HT}(s) = \frac{1 - sT_W}{1 + 0.5sT_W} \tag{5}$$

where, T_W is the hydro turbine time constant.

The power outputs of these units are sent to the input of the generator, which is used to generate electricity for the power system. The generator is represented by the transfer function

$$G_P(s) = \frac{K_P}{1 + sT_P} \tag{6}$$

where, K_P is the power system gain constant, T_P is the power system time constant.

The tie-line power deviation

$$\Delta P_{tie12} = \frac{2\pi T_{12}}{s}(\Delta F_1 - \Delta F_2) \tag{7}$$

where, T_{12} is the tie-line synchronizing coefficient, ΔF_1 and ΔF_2 are the frequency deviation of area-1 and area-2 respectively.

B. MODELING OF THE CAPACITIVE ENERGY STORAGE

CES devices have great potential in modern power system. They have the potential to alleviate low-frequency power fluctuations and to stabilize system frequency deviations due to system transients. They can improve the stability of hybrid power system. CES devices have various advantages such as fast charging/discharging rate without loss of efficiency, small response time, high power density, long working life, large capacity to supply high frequency power demand into the grid, easy maintenance, environment friendly, simple operation and low cost [28], etc.

A CES unit consists of a capacitor, a power conversion system (PCS), and a protection circuit. The CES unit stores energy in capacitors in the form of electrostatic charge under normal operating conditions and releases it instantaneously

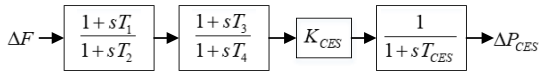

FIGURE 3. Transfer function model of CES applied to AGC [12], [28].

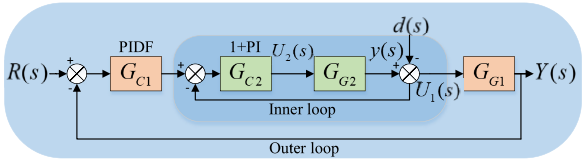

FIGURE 4. Block diagram of the traditional cascade controller [16].

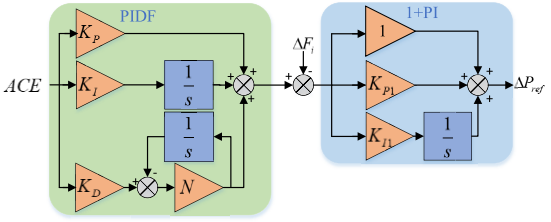

FIGURE 5. PIDF-(1+PI) cascade controller.

into the grid via PCS during sudden changes in load demand. Hence, the governors and other control devices in the power system come into play to regulate the power to reach a new balance. The energy efficiency of CES devices is about 95%. The main losses are caused by PCS, internal leakage, and self-discharge. Therefore, CES can help AGC to quickly regulate the power system to the new equilibrium steady-state condition effectively, and is an excellent energy storage device to enhance the stability of the AGC system. In the AGC system, both frequency deviation ΔF and area control error (ACE) can be used as the control signal of the CES device. In this paper, frequency deviation is selected as the control signal of the CES device. To enhance the dynamic performance of the power system and to mitigate frequency deviation and tie-line power deviation, CES units are integrated into all areas of the power system model. The incremental change in power of the CES unit is given as [28]

$$\Delta P_{CESi} = \left\{ \left[\frac{1+sT_1}{1+sT_2} \right] \left[\frac{1+sT_3}{1+sT_4} \right] \left[\frac{K_{CES}}{1+sT_{CES}} \right] \right\} \Delta F_i \quad (8)$$

where, $i = 1,2$. T_1, T_2, T_3 and T_4 are the time constants of two-stage phase compensation blocks. K_{CES} is the gain of CES unit and T_{CES} is the time constant of CES unit. The ΔF_i is the frequency deviation signal for area-i. The ΔF_i of each area is used as an input-controlled variable to the CES unit to provide the required power.

III. PIDF-(1+PI) CASCADE CONTROLLER

The concept of cascade control refers to the control of two consecutive processes where the output of the inner process supplies the outer process in sequence. The main purpose of introducing a cascade controller is to resist load perturbations quickly and prevent them from spreading to other parts of the system effectively. The cascade controller consists of two loops, an outer loop and an inner loop corresponding to the external process and the internal process, respectively. The cascade controller offers greater advantages than a normal controller in that it improves response time and minimizes system perturbations by performing corrections within the system model. Fig.4 shows the model of a traditional two-loop cascade controller.

The outer loop of the cascade controller controls the absolute response $Y(s)$ of the system and is therefore called the master or main control. $G_{G1}(s)$ is the outer process gain. $d(s)$ is the load perturbation to which the system is subjected. The output of the outer loop is equated to the reference signal to drive the system to stabilization. $G_{C1}(s)$ is the outer loop controller. $U_1(s)$ is the input signal of $G_{G1}(s)$ in the outer loop and also the output of the inner loop. The outer loop control is primarily designed to measure and control the quality of the final output of the overall control process. The inner loop, also known as the slave or secondary loop, uses the outputs of $U_1(s)$ and $G_{C1}(s)$ as inputs to the inner loop controller $G_{C2}(s)$. $U_2(s)$ is the output of the inner loop controller $G_{C2}(s)$ and the input signal of the inner gain $G_{G2}(s)$ in the inner loop. $Y(s)$ is the output of $G_{G2}(s)$. The inner loop control is mainly to attenuate the effect of perturbations or any inner process perturbations on the outer process.

The traditional two-loop cascade controller is represented by

$$\begin{aligned} Y(s) &= \left[\frac{G_{G1}(s)G_{G2}(s)G_{C1}(s)G_{C2}(s)}{1+G_{G2}(s)G_{C2}(s)+G_{G1}(s)G_{G2}(s)G_{C1}(s)G_{C2}(s)} \right] R(s) \\ &\quad - \left[\frac{G_{G1}(s)}{1+G_{G2}(s)G_{C2}(s)+G_{G1}(s)G_{G2}(s)G_{C1}(s)G_{C2}(s)} \right] d(s) \end{aligned} \quad (9)$$

where, R(s) is the reference signal, and d(s) is the perturbation signal.

In this paper, a PIDF-(1+PI) cascade controller is designed with the structure shown in Fig.5. It has the merits of classical PID controllers such as good performance, understandable structure, and convenient debugging in engineering applications. It consists of dual control loops (i.e., inner and outer loops). Its inner loop controller can reduce the equivalent time constant of the controlled object, improve the response speed, and effectively suppress the perturbation of the internal loop of the system. Its outer loop controller effectively suppresses the perturbation of the external loop of the system, improves the control robustness, and ensures the achievement of the control objectives. The outer-loop controller is a PIDF controller and the inner-loop controller is a (1+PI) controller. The (1+PI) controller combines the controller input with the PI controller output to effectively limit the effect of load perturbations variations on the system and improve the efficiency of the control [33]. Moreover, since the two controllers are incorporated in a cascade connection, it tends to reject perturbations more quickly before they spread out in the system [13].

The transfer functions of the PIDF controller and 1+PI controller are

$$G_{PIDF}(s) = K_P + \frac{K_I}{s} + \frac{K_D N s}{s+N} \tag{10}$$

$$G_{1+PI}(s) = 1 + K_{P1} + \frac{K_{I1}}{s} \tag{11}$$

where, K_P, K_I, K_D and N are proportional, integral, derivative and derivative filter gains of PIDF controller, respectively. K_{P1}, K_{I1} are proportional, integral of 1+PI controller.

The input of the outer-loop controller is the *ACE* of the AGC system. The ΔF_i and outer-loop controller are the input of the inner-loop controller. For each area, the tie-line bias control (TBC) mode is used, and the equations of *ACE* for area-1 and area-2 are

$$ACE_1 = B_1 \Delta F_1 + \Delta P_{tie12} \tag{12}$$

$$ACE_2 = B_2 \Delta F_2 + \alpha_{12} \Delta P_{tie12} \tag{13}$$

where, B_1, B_2 are the frequency response characteristics of area-1 and area-2.

In order to simplify the analysis, this paper assumes that the two areas are identical and also the controller parameters are identical. The output ΔP_{refi} of the controller in area-*i* is

$$\Delta P_{refi} = \left(ACE_i \left(K_P + \frac{K_I}{s} + \frac{K_D N s}{s+N} \right) - \Delta F_i \right) \times \left(1 + K_{P1} + \frac{K_{I1}}{s} \right) \tag{14}$$

IV. CONTROLLER PARAMETER OPTIMIZATION

For the designed controller, the parameters of the controller need to be optimized. Suitable controller parameters will lead to better performance of the power system. This section describes in detail the parameter optimization algorithm and objective function used in this paper.

A. THE WHALE OPTIMIZATION ALGORITHM

The WOA originates from the simulation of the unique spiral bubble-feeding behavior of humpback whales in nature. It is assumed that the current best individual is the prey, and the other individuals in the group all approach the best individual. WOA achieves the purpose of optimized search through the process of encircling prey, the bubble-net attacking method, and search for prey. WOA is mainly divided into three stages: exploration phase (search for prey), encircling prey phase, and the bubble-net attacking phase.

The selection of the three phases of the exploration phase, encircling prey, and exploitation phase is determined by the value of the probability factor p and the coefficient |A|. When $p < 0.5$, the exploration phase and encircling prey phase are entered.

When $|A| \geq 1$, the whale individual enters the exploration phase. Whale individuals perform a random search based on their respective relative positions. The exploration phase is a process in which whales randomly search for prey, and whale individuals perform random searches based on their positions to each other, corresponding to the global search phase of the algorithm, whose mathematical model is expressed as

$$D = |CX_R(m) - X(m)| \tag{15}$$

$$X(m+1) = X_R(m) - AD \tag{16}$$

where, $X_R(m)$ is a random position vector (a random whale) chosen from the current population. $X(m)$ is the position vector. m is the number of iterations. D is the step length. A and C are the coefficient vectors and are defined as

$$A = 2ar_1 - a \tag{17}$$

$$C = 2r_2 \tag{18}$$

where, r_1 and r_2 are random numbers between [0, 1]. a is called the control parameter that decreases linearly from 2 to 0 with the increasing number of iterations. a is given by

$$a = 2 - \frac{2m}{Maxi} \tag{19}$$

where, *Maxi* is the maximum number of iterations.

The encircling prey phase, and bubble-net attacking phase correspond to the partial exploitation phase of the algorithm. When $|A| < 1$, the whale individual will approach the position of the best solution obtained so far. This is the time to enter the encircling prey phase. The mathematical model of the encircling prey phase is expressed as

$$D_b = |CX_{best}(m) - X(m)| \tag{20}$$

$$X(m+1) = X_{best}(m) - AD_b \tag{21}$$

where, $X_{best}(m)$ is the position vector of the best solution obtained so far and defined as search agent. D_b is the enclosing step length. The larger $|A|$ is, the larger the step length the whale swims. Fig.6(a) translates Eqn. (21) into a 2D space chart to illustrate the operation principle. The individual position coordinates (X, Y) are updated in position according to the optimal position coordinates (X_{best}, Y_{best}). By adjusting the values of the coefficient vectors A and C, the control of the current position can be achieved at different locations around the best position. The possibility of position search to update the position in 3D space is shown in Fig.6(b). The (X_{best}, Y_{best}) and $(X_{best}, Y_{best}, Z_{best})$ are the best solutions obtained so far in 2D space and 3D space, respectively.

Fig.7 shows how the exploration phase and encircling prey phase are implemented when A is greater than 1 or less than 1. Fig.7 shows the possible locations of some specific solutions when $|A| > 1$ or the locations of individuals with $|A| < 1$ in the vicinity of the current optimal location.

When $p \geq 0.5$, it enters the bubble-net attacking phase. Whale individual will approach the best individual position obtained so far. The whale individual swim for food in a spiral, searching for the best possible solution between individual whales and the best individual. The initial point is the position of the current whale individual. The target endpoint is the position of the current best whale individual. The

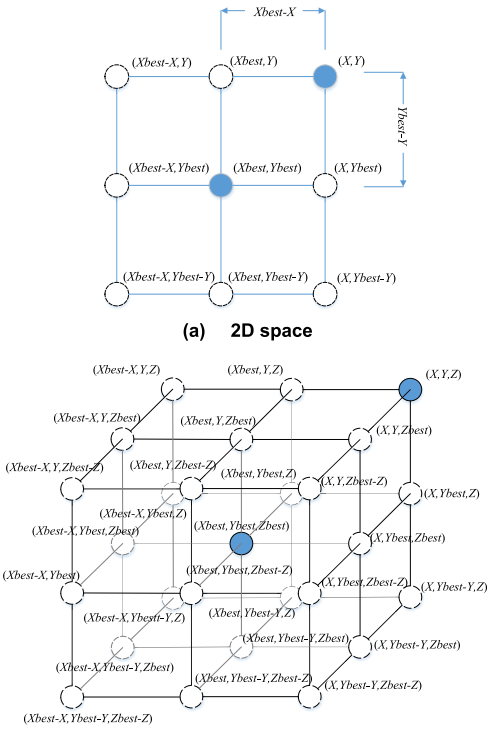

FIGURE 6. Position vectors and their possible next locations [27].

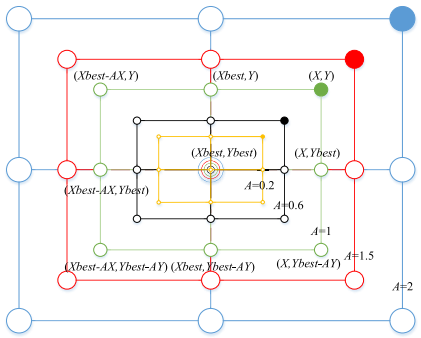

FIGURE 7. Exploration mechanism and shrinking encircling mechanism [27].

mathematical model can be expressed as

$$D_d = |X_{best}(m) - X(m)| \tag{22}$$

$$X(m+1) = X_{best}(m) + D_d e^{bl} \cos(2\pi l) \tag{23}$$

where, D_d is the distance between the current individual whale and the current best whale individual. b is a constant for defining the shape of the logarithmic spiral, l is a random number in $[-1,1]$.

B. WOA-W

The complexity of the power system model places great demands on the optimization algorithm's optimization-seeking capability and the algorithm's running time. WOA has a strong optimization-seeking capability, while its simple mechanism enables parameter optimization in a relatively short period of time even in the face of complex power system. But the traditional WOA has disadvantages such as slow convergence and easy to fall into local optimum [34]. To overcome these disadvantages and make the algorithm more suitable for AGC in power system, in this paper, a modified WOA improved by nonlinear time-varying adaptive weight (WOA-w) is proposed.

WOA enters the exploration phase when $|A| \geq 1$. The search range needs to be expanded as much as possible. Larger A values allow whale individual to maintain a better exploratory capacity. When $|A| < 1$, WOA tries to achieve a higher optimization accuracy in finding the optimal solution based on the position of the best solution. Smaller A will correspond to better partial exploitation capacity. The variation of A directly affects the exploratory capacity and partial exploitation capacity at different stages. In the traditional WOA, the size of A is determined by the control parameter a. Inspired by [25] and [26], a nonlinear time-varying adaptive weight (ω) is introduced to control the change in the size of a. ω is defined as

$$\omega = \frac{1}{2}\left[1 + \cos\left(\frac{\pi m}{Maxi}\right)\right]^{\frac{1}{k}} \tag{24}$$

where, k is the adjustment factor.

At the beginning of the algorithm iteration, the weight factor is large. The algorithm can maintain a good global search capability. After a certain number of iterations, the weight factor decreases rapidly. The algorithm can jump out of the local optimum and further improve the optimization accuracy.

Eqns. (16) and (23) are updated to Eqns. (25) and (26) after the introduction of the new nonlinear time-varying adaptive weight

$$X(m+1) = X_R(m) - \omega AD \tag{25}$$

$$X(m+1) = X_{best}(t) + \omega D_d e^{bl} \cos(2\pi l) \tag{26}$$

Fig.8 shows the pseudo-code for WOA-w.

C. PERFORMANCE ANALYSIS OF ALGORITHM

To verify the solution performance of WOA-w, some standard benchmark functions are selected for comparative simulation test. Table 1 shows the benchmark functions selected in this paper [27]. For these benchmark functions, WOA shows good solution performance in some functions and poor solution performance in others. This is caused by the inherent advantages and disadvantages of WOA. F_1 is unimodal function. F_2 and F_3 are multimodal functions. These functions are used by many researchers to verify the exploration and exploitation capability of algorithms. Table 1 consists of four columns: the benchmark functions, the number of design variables(V_no), range of variation of optimization variables, and the optimal value $f_{\min}$ quoted in literature. Applying the WOA-w to the solution of the benchmark functions, the results are compared with those of WOA and GWO. For all the algorithms, a population size and maximum iteration equal to 30 and 500 have been utilized, respectively.

TABLE 1. Benchmark functions.

Function	V_no	Range	f_{min}
$F_1(x)=\sum_{i=1}^{n} ix_i^4+random[0,1)$	30	[-1.28,1.28]	0
$F_2(x)=\frac{\pi}{n}\left\{10\sin(\pi y_1)+\sum_{i=1}^{n-1}(y_i-1)^2\left[1+10\sin^2(\pi y_{i+1})+(y_n-1)^2\right]\right\}+\sum_{i=1}^{n}u(x_i,10,100,4)$			
$y_i=1+\frac{x_i+1}{4}$, $u(x_i,a,k,m)=\begin{cases}k(x_i-a)^m, x_i>a\\0,-a<x_i<a\\k(-x_i-a)^m, x_i<-a\end{cases}$	30	[-50,50]	0
$F_3(x)=\sum_{i=1}^{11}\left[a_i-\frac{x_1(b_i^2+b_ix_2)}{b_i^2+b_ix_3+x_4}\right]^2$	4	[-5,5]	0.00030

TABLE 2. Comparison of optimization results obtained for the benchmark functions.

F	WOA-w		WOA		GWO	
	ave	std	ave	std	ave	std
F_1	7.824×10^{-4}	9.422×10^{-4}	1.822×10^{-3}	1.731×10^{-3}	4.381×10^{-3}	3.805×10^{-3}
F_2	0.0380	0.0129	0.0834	0.0285	0.0302	0.0225
F_3	5.021×10^{-4}	2.937×10^{-4}	7.495×10^{-4}	3.819×10^{-4}	1.095×10^{-3}	6.423×10^{-4}

```
Initialize the whales population Xi (i = 1, 2, ..., n)
Calculate the fitness of each search agent
Xb=the best search agent
while (t < maximum number of iterations)
    for each search agent
    Update a, A, C, l, and p
    Update the value of ω by the Eqn. (24)
        if1 (p<0.5)
            if2 (|A| < 1)
                Update the position of the current search agent by the Eqn. (21)
            else if2 (|A| ≥1)
                Select a random search agent (XR )
                Update the position of the current search agent by the Eqn. (25)
            end if2
        else if1 (p ≥0.5)
                Update the position of the current search by the Eqn. (26)
        end if1
    end for
    Check if any search agent goes beyond the search space and amend it
    Calculate the fitness of each search agent
    Update Xb if there is a better solution
    t=t+1
end while
return Xb
```

FIGURE 8. The pseudo-code for WOA-w.

The statistical results of average and standard deviations are gathered in the Table 2. F1 is a unimodal function. It has only one global optimum. This function allows to evaluate the exploitation capability of the investigated metaheuristic algorithms [27]. For F1 it can be seen that WOA-w has a better exploration capability. F2 and F3 are multimodal functions. They include many local optima whose number increases exponentially with the problem size (number of design variables). This type of function is often used to evaluate the exploratory search capability of an algorithm [27]. It can be seen that the traditional WOA performance is weaker than GWO from F2. This is mainly due to the slow convergence speed of the WOA17. WOA-w accelerates the convergence speed by the ω, which greatly reduces the performance gap between WOA and GWO on this class of functions. For F2 and F3, it can be seen that WOA-w has the same good performance in handling multimodal functions. This shows that WOA-w has a good development capability. The convergence curves of the optimal results for WOA-w, WOA and GWO for the three benchmark functions are given in Fig.9. It can be seen from Fig. 9 that WOA-w has better convergence properties.

D. OBJECTIVE FUNCTION AND OPTIMIZATION CONSTRAINTS

When performing controller parameter optimization, it is first necessary to define the objective function according to the required specifications and constraints. The design of objective function to tune controller parameters requires consideration of the performance criteria of the entire closed loop response. The parameter optimization problem of the PIDF-(1+PI) cascade controller can be formulated as a search for appropriate values of K_P, K_I, K_D, N, K_{P1}, K_{I1} in a certain range that the objective function is minimized. Commonly used performance criteria in industry are integral squared error (ISE), integral of time multiplied squared error (ITSE), integral absolute error (IAE) and integral of time multiplied absolute error (ITAE) [35]. As ITSE penalizes squared error and IAE give importance to only absolute error, these criteria are not often used as objective function in controller design. ISE integrates the square of the error over time, the square of the larger error will be larger, so the larger error receives more penalty than the smaller error [36]. The system tends to eliminate large errors quickly in order to minimize ISE, but this can lead to the presence of smaller errors for a long period of time. This usually results in a system with a fast response, but still

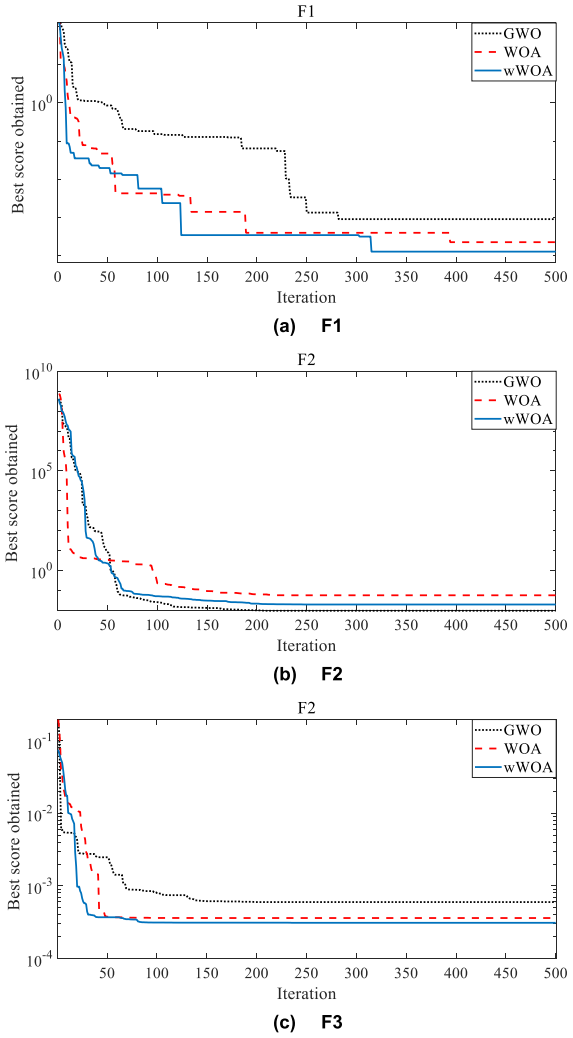

FIGURE 9. Comparison of best convergence curves of WOA-w and other algorithms obtained in the benchmark problems.

with a small oscillation after stabilization. ITAE integrates the absolute error multiplied by the time over time, hence penalties for errors that exist after a long time are much more heavily than those at the beginning of the response – [36]. Therefore, the control method using ITAE is more stable than using ISE. This indicates that ITAE is the most appropriate objective function in the AGC design, and therefore ITAE is selected as the objective function in this paper. In this paper, the WOA-w is used as the optimization algorithm, and ITAE is used as the objective function to establish an optimal model for the PIDF-(1+PI) cascade controller of the AGC. The ISE, ITSE, and IAE are also used as references for comparison. The objective function J is given by

$$J = \int_0^T t(|\Delta F_1| + |\Delta F_2| + |\Delta P_{tie12}|)dt \tag{27}$$

the other three criteria are given by

$$\text{ISE} = \int_0^T \left(\Delta F_1^2 + \Delta F_2^2 + \Delta P_{tie12}^2\right)dt \tag{28}$$

TABLE 3. System parameters [12], [32].

Parameter	Numerical values	Parameter	Numerical values
α_{12}	-1	T_1	0.279s
P_{r1}	1000 puMW	T_2	0.026s
P_{r2}	1000 puMW	T_3	0.411s
T_G	0.08s	T_4	0.1s
T_T	0.3s	K_{CES}	0.3
K_R	1	T_{CES}	0.0352
T_{RH}	48.7s	B_1, B_2	0.425puMW/Hz
T_R	5s	R_1	2.0Hz/pu
T_{GH}	0.513s	R_2	2.4Hz/pu
T_W	1s	$Maxi$	100
K_P	100 Hz/puMW	K	30
T_P	20S	k	0.5
T_{12}	0.0707 pu/rad		

$$\text{ITSE} = \int_0^T t\left(\Delta F_1^2 + \Delta F_2^2 + \Delta P_{tie12}^2\right)dt \tag{29}$$

$$\text{IAE} = \int_0^T (|\Delta F_1| + |\Delta F_2| + |\Delta P_{tie12}|)dt \tag{30}$$

where, J is the ITAE criterion value, T is the simulation time.

For the PIDF-(1+PI) cascade controller, the constraint is

$$\text{s.t.} \quad \begin{cases} K_P^{\min} \le K_P \le K_P^{\max} \\ K_I^{\min} \le K_I \le K_I^{\max} \\ K_D^{\min} \le K_D \le K_D^{\max} \\ N^{\min} \le N \le N^{\max} \\ K_{P1}^{\min} \le K_{P1} \le K_{P1}^{\max} \\ K_{I1}^{\min} \le K_{I1} \le K_{I1}^{\max} \end{cases} \tag{31}$$

where, K_P^{min}, K_P^{max}, K_I^{min}, K_I^{max}, K_D^{min}, K_D^{max}, N^{min}, N^{max} are the minimum and maximum values of proportional, integral, derivative and derivative filter gains of PIDF controller, respectively. K_{P1}^{min}, K_P^{max}, K_{I1}^{min}, K_{I1}^{max} are the minimum and maximum values of proportional, integral of 1+PI controller, respectively.

V. SIMULATION RESULTS

A. SIMULATION PARAMETER SETTING

A two-area multi-unit multi-source hydro/thermal power system with CES is built in MATLAB /Simulink environment. The values of the initial parameters of the WOA-w should be selected reasonably according to the complexity of the objective function and the size of the search space. According to the established optimization model and the range of values of optimization variables, combined with relevant simulation experience and other references on the optimization of AGC controller parameters using metaheuristic algorithm optimization algorithms, a more reasonable set of values for the initial WOA-w parameters selected in this paper are: the population size $K = 30$, maximum iteration $Maxi = 100$, the adjustment factor $k = 0.5$. K_P, K_I, K_D, K_{P1}, K_{I1} take values in the range $[-5, 5]$, and N takes values in the range $[1, 200]$. Table 3 shows the specific system simulation parameters, which refer to [12] and [32].

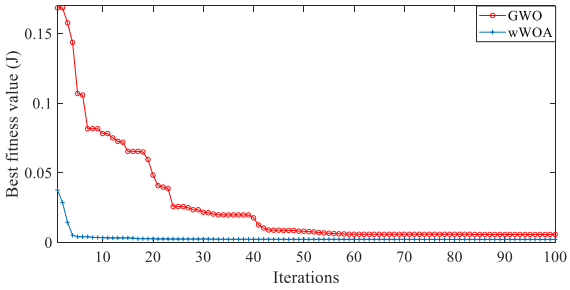

FIGURE 10. Comparison of best convergence curves of WOA-w and GWO.

TABLE 4. Controller parameters.

	WOA-w Cascade PIDF-(1+PI)	GWO Cascade PIDF-(1+PI)	hSFS-LUS PDF-(1+PI)	FA PID
K_P	4.9881	-3.1852	-4.8565	-4.9750
K_I	-0.0280	-3.2886		-4.9750
K_D	3.7737	-1.8436	-1.3012	-1.5410
N	34.4350	23.3787	45.5235	
K_{P1}	-2.4111	0.8459	0.1213	
K_{I1}	-5.0000	2.3073	2.3212	

Assuming that a step load perturbation (SLP) of 0.01 puMW occurs in area-1, the power system is controlled by a PIDF-(1+PI) cascade controller. And the WOA-w is run in MATLAB to optimize the controller parameters according to the objective function J. The WOA-w is run thirty times, and the optimal results are selected as the controller parameters in the nominal condition. Fig.10 shows the convergence curve corresponding to the best fitness value of WOA-w. In order to verify the superiority of WOA-w for the optimization of AGC controller parameters, GWO is selected to optimize the parameters of the PIDF-(1+PI) cascade controller. The convergence curves corresponding to the best fitness value of GWO are also given in Fig.10.

From Fig.10, WOA-w has a faster convergence speed and a higher search accuracy compared to GWO. WOA-w can convert in the exploration phase and exploitation phase of the algorithm by the weight factor ω which speeds up the convergence speed and improves the search accuracy. To verify the superiority of PIDF-(1+PI) cascade controller for AGC, two control strategies, hSFS-LUS optimized PDF-(1+PI), and FA optimized PID, are selected for comparison.

Table 4 shows the optimized controller parameters of the four control strategies.

B. SIMULATION ANALYSIS

To verify the performance of the proposed control strategy, two simulation cases are implemented. Case 1 assumes that SLP=0.01puMW in area-1. It analyzes the performance of the proposed WOA-w optimized PIDF-(1+PI) cascade controller by the responses of ΔF_1, ΔF_2, ΔP_{tie}, area-1 power generation(ΔP_{g1}), and area-2 power generation(ΔP_{g2}). To verify the sensitivity of the proposed controller, case 2 assumes that SLP = 0.01puMW in area-1 and SLP = 0.05puMW in area-2. It should be noted that for ΔF_1, ΔF_2, ΔP_{tie}, ΔP_{g1} and ΔP_{g2}, the tolerance range at the final stabilization at the value of 0 is [−0.0001,0.0001]. For all case studies, the four engineering criteria ITAE, ITSE, IAE, and ISE are calculated by taking a simulation time of 15 s.

1) CASE1: LOAD PERTURBATION OCCURS IN AREA-1

Fig.11 and Table 5 show the dynamic response of the system when SLP = 0.01puMW in area-1(ΔP_{D1} = 0.01puMW). Fig. 11 and Table 5 show that compared with the three control strategies of GWO optimized PIDF-(1+PI) cascade controller, hSFS-LUS optimized PDF-(1+PI), and FA optimized PID, the proposed WOA-w optimized PIDF-(1+PI) cascade controller has the minimum J (ITAE = 2.3×10^{-3}), which is reduced by 60.34%, 65.67%, and 80.83% compared to the other three comparison control strategies, the shortest settling time (St, $\mathrm{St}_{F1} = 1.354$s, $\mathrm{St}_{F2} = 2.455$s, $\mathrm{St}_{Ptie} = 0.955$s). The settling time of ΔF_1 is reduced by 59.75%, 55.97%, 21.55% compared to the other three comparison control strategies. The settling time of ΔF_2 is reduced by 49.53%, 18.87%, 18.84% compared to the other three comparison control strategies. The settling time of ΔP_{tie} is reduced by 75.21%, 66.68%, 58.80% compared to the other three comparison control strategies. Meanwhile, the maximum frequency deviation of area-1 and area-2 are -2.1×10^{-3} Hz and -6.8×10^{-4} Hz, respectively. And the maximum power deviation of the contact line is -2.0×10^{-4}puMW, which is smaller than the maximum deviation of the other three comparison control strategies. The ITSE, IAE, and ISE are 3.8×10^{-7}, 1.8×10^{-3}, and 1.1×10^{-6}, respectively, which are significantly smaller than the other three comparison control strategies. The ITSE is reduced by 65.45%, 86.43%, and 91.56% compared to the other three comparison control strategies. The IAE is reduced by 41.94%, 60%, and 72.73% compared to the other three comparison control strategies. The ISE is reduced by 52.38%, 76.27%, and 86.25% compared to the other three comparison control strategies.

To show the superiority of the proposed control strategy more clearly, the simulation results are extended by introducing the responses of the power generation in area-1 (ΔP_{g1}) and the power generation in area-2 (ΔP_{g2}) in Fig. 11 and Table 5. ΔP_{g1} reaches the required 0.01puMW at 1.705s, which is 54.75%, 55.77%, and 30.75% shorter than the other three control strategies, respectively; ΔP_{ge2} returns to the zero position at 1.656s, which is 31.14%, 56.83%, and 36.25% shorter than the other three control strategies, respectively.

In summary, the proposed control strategy can effectively make the system frequency deviations and tie-line power deviation return to zero quickly, and reduce the five settling times by 40.05% on average compared to the other three comparison control strategies. At the same time, it has better dynamic responses compared with the other three comparison control strategies. The ITAE, maximum frequency deviation in area-1, maximum frequency deviation in area-2, and maximum power deviation in the tie-line are significantly smaller than the other three comparison control strategies.

TABLE 5. Numerical values of system response at $\Delta P_{D1} = 0.01$puMW.

		WOA-w Cascade PIDF-(1+PI)	GWO Cascade PIDF-(1+PI)	hSFS-LUS PIDF-(1+PI)	FA PID
ITAE		2.3×10^{-3}	5.8×10^{-3}	6.7×10^{-3}	0.012
ITSE		3.8×10^{-7}	1.1×10^{-6}	2.8×10^{-6}	4.5×10^{-6}
IAE		1.8×10^{-3}	3.1×10^{-3}	4.5×10^{-3}	6.6×10^{-3}
ISE		1.1×10^{-6}	2.1×10^{-6}	5.9×10^{-6}	8.0×10^{-6}
Settling time(s)	ΔF_1	1.354	3.364	3.075	1.726
	ΔF_2	2.455	4.864	3.026	3.025
	ΔP_{tie}	0.955	3.852	2.866	2.318
	ΔP_{g1}	1.705	3.768	3.855	2.462
	ΔP_{g2}	1.656	2.405	3.836	2.598
Max.frequency diviation(Hz)	ΔF_1	-2.1×10^{-3}	-2.7×10^{-3}	-3.5×10^{-3}	-3.5×10^{-3}
	ΔF_2	-6.8×10^{-4}	-8.3×10^{-4}	-1.7×10^{-3}	-1.8×10^{-3}
Max.power diviation(puMW)	ΔP_{tie}	-2.0×10^{-4}	-3.3×10^{-4}	-6.0×10^{-4}	-7.2×10^{-4}

TABLE 6. Numerical values of system response at $\Delta P_{D1} = 0.01$puMW and $\Delta P_{D2} = 0.05$puMW.

		WOA-w Cascade PIDF-(1+PI)	GWO Cascade PIDF-(1+PI)	hSFS-LUS PIDF-(1+PI)	FA PID
ITAE		0.013	0.030	0.032	0.063
ITSE		1.2×10^{-5}	2.9×10^{-5}	6.2×10^{-5}	1.4×10^{-4}
IAE		0.010	0.016	0.022	0.033
ISE		3.0×10^{-5}	5.5×10^{-5}	1.5×10^{-4}	2.4×10^{-4}
Settling time(s)	ΔF_1	4.663	6.503	7.949	/
	ΔF_2	4.726	4.760	7.407	/
	ΔP_{tie}	1.795	5.126	2.741	3.018
	ΔP_{g1}	1.949	4.762	5.382	3.593
	ΔP_{g2}	2.306	5.082	7.148	6.318
Max.frequency diviation(Hz)	ΔF_1	-3.3×10^{-3}	-4.0×10^{-3}	-7.8×10^{-3}	-9.6×10^{-3}
	ΔF_2	-0.010	-0.013	-0.018	-0.018
Max.power diviation(puMW)	ΔP_{tie}	8.1×10^{-4}	1.3×10^{-3}	2.4×10^{-3}	2.9×10^{-3}

TABLE 7. Numerical values of system response when hydro parameter is changed.

		Nominal Parameter	-25% of Nominal Hydro Parameter	+25% of Nominal Hydro Parameter
ITAE		2.3×10^{-3}	2.6×10^{-3}	2.2×10^{-3}
Settling time(s)	ΔF_1	1.354	1.831	1.354
	ΔF_2	2.455	2.539	2.435
	ΔP_{tie}	0.955	0.935	0.982
	ΔP_{g1}	1.705	1.721	1.671
	ΔP_{g2}	1.656	1.702	1.584
Max.frequency diviation(Hz)	ΔF_1	-2.1×10^{-3}	-2.1×10^{-3}	-2.0×10^{-3}
	ΔF_2	-6.8×10^{-4}	-7.2×10^{-4}	-6.5×10^{-4}
Max.power diviation(puMW)	ΔP_{tie}	-2.0×10^{-4}	-2.1×10^{-4}	-2.0×10^{-4}

2) CASE2: LOAD PERTURBATIONS OCCUR IN AREA-1 AND AREA-2

Fig. 12 and Table 6 show the dynamic response of the system when SLP = 0.01puMW in area-1(ΔP_{D1} = 0.01puMW) and SLP = 0.05puMW in area-2(ΔP_{D2} = 0.05puMW). Fig. 12 and Table 6 show that compared with the three control strategies of GWO optimized PIDF-(1+PI) cascade controller, hSFS-LUS optimized PDF-(1+PI), and FA optimized PID, the proposed WOA-w optimized PIDF-(1+PI) cascade controller has the minimum J (ITAE=0.013), which is reduced by 56.67%, 59.38%, and 79.37% compared to the other three comparison control strategies, and the shortest settling time (St_{F1} = 4.663s, St_{F2} = 4.726s, St_{Ptie} = 1.795s). The settling time of ΔF_1 is reduced by 28.29%, 41.34%

TABLE 8. Settling time for each time period when random SLP occur in area-1 and area-2.

		0-20s	20-40s	40-60s	60-80s	80-100s
WOA-w	ΔF_1	4.865	25.146	44.943	65.636	84.545
Cascade	ΔF_2	4.875	25.121	45.018	62.847	84.537
PIDF-(1+PI)	ΔP_{tie}	1.626	21.806	41.644	61.446	80.950
GWO	ΔF_1	5.449	25.952	56.431	67.025	86.333
Cascade	ΔF_2	6.521	26.758	46.017	67.033	86.046
PIDF-(1+PI)	ΔP_{tie}	4.963	25.129	44.966	64.672	83.848
hSFS-LUS	ΔF_1	7.483	26.567	59.853	75.604	99.084
PIDF-(1+PI)	ΔF_2	8.034	27.109	59.737	75.515	98.984
	ΔP_{tie}	2.239	22.759	42.182	61.863	81.740
	ΔF_1	\	\	\	\	\
FA PID	ΔF_2	\	\	\	\	\
	ΔP_{tie}	2.861	23.049	42.941	62.754	82.286

compared to the first two comparison control strategies. The settling time of ΔF_2 is reduced by 0.71%, 36.20% compared to the first two comparison control strategies. The settling time of ΔP_{tie} is reduced by 64.98%, 34.51%, and 40.52% compared to the other three comparison control strategies. Meanwhile, the maximum frequency deviations of area-1 and area-2 are -3.3×10^{-3}Hz and -0.010Hz, respectively, and the maximum power deviation of the tie-line is 8.1×10^{-4}pu, which is smaller than the maximum deviation of the other three comparison control strategies. The ITSE, IAE, and ISE are 1.2×10^{-5}, 0.010, and 3.0×10^{-5}, respectively, which are significantly smaller than the other three comparison control strategies. The ITSE is reduced by 58.62%, 80.65%, and 91.43% compared to the other three comparison control strategies. The IAE is reduced by 37.5%, 54.55%, and 67.70% compared to the other three comparison control strategies. The ISE is reduced by 45.45%, 80%, and 87.5% compared to the other three comparison control strategies. Since the SLP in area-2 is larger than in area-1, the maximum frequency deviation in area-2 is larger than that of in area-1. Specifically, for the GA optimized PID controller, ΔF_1 and ΔF_2 fail to stabilize within the tolerance range within 15s, but within $[-0.001, 0.001]$.

To show the superiority of the proposed control strategy more clearly, the simulation results are extended by introducing the responses of the power generation in area-1 (ΔP_{g1}) and the power generation in area-2 (ΔP_{g2}) in Fig. 12 and Table 6. ΔP_{g1} reaches the required 0.01puMW at 1.949s, which is 59.07%, 63.78%, and 45.76% shorter than the other three control strategies, respectively; ΔP_{g2} returns the required 0.01puMW at 2.306s, which is 54.62%, 67.74%, and 63.50% shorter than the other three control strategies, respectively.

In summary, the proposed control strategy can effectively make the system frequency deviations and tie-line power deviation return to zero quickly when the SLP change, and reduce the five settling times by 46.23% on average compared to the other three comparison control strategies. This indicates that the proposed control strategy is highly sensitive to resist perturbation variations in the system. At the same time, it has a better dynamic response compared with the other three comparison control strategies. The ITAE, maximum frequency deviation in area-1, maximum frequency deviation in area-2, and maximum power deviation in the tie-line are significantly smaller than the other three comparison control strategies.

According to the simulation results of the above two cases, the controller parameters optimized by the WOA-w can make the proposed controller achieve the desired performance. The proposed controller is able to suppress the frequency deviations in each area and tie-line power deviation to zero in the shortest time, and it has the best dynamic response compared with other three control strategies. Each of the performance indicators of the proposed control strategy is optimal. When the SLP change from case 1 to case 2, the dynamic response of hSFS-LUS optimized PDF-(1+PI), and FA optimized PID changes greatly, and the performance of some indicators show a certain degree of weakening. The dynamic response of the GWO optimized PIDF-(1+PI) cascade controller is more stable. This also illustrates the superior performance of the PIDF-(1+PI) cascade controller.

VI. ROBUSTNESS ANALYSIS

The proposed WOA-w optimized PIDF-(1+PI) cascade controller designed under nominal system condition should be robust at changing system conditions. The proposed controller should be able to achieve the desired dynamic performance under different operating conditions. In order to verify the robustness of the proposed controller, three cases are designed for verification. Case 3 is to change the system hydro unit parameters, Case 4 is to set a random SLP in the system, and Case 5 is to set the nonlinearity effects in the system.

A. VARIATION IN SYSTEM PARAMETERS

The system parameters usually change with time or deviations in the system structure. The controller designed under nominal conditions must be robust enough to withstand changes of system parameters in an interconnected power system. Assuming SLP=0.01puMW in area-1, the hydro unit parameters are varied by ±25% from the nominal values. Fig.13 and Table 7 show the response performance of the proposed control strategy when the hydro unit parameters are

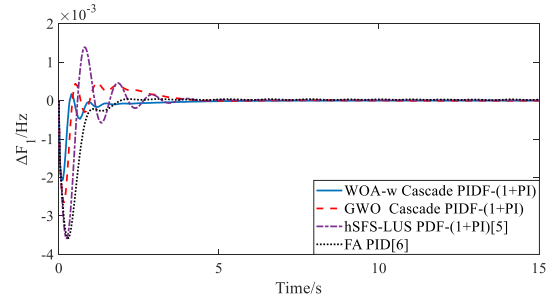

(a) ΔF_1

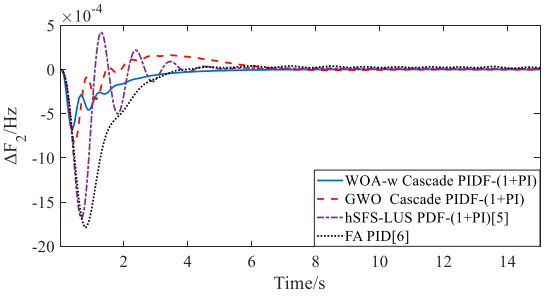

(b) ΔF_2

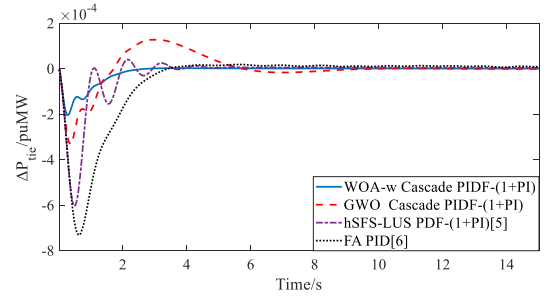

(c) ΔP_{tie}

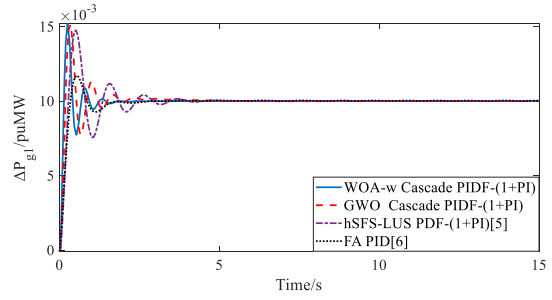

(d) ΔP_{g1}

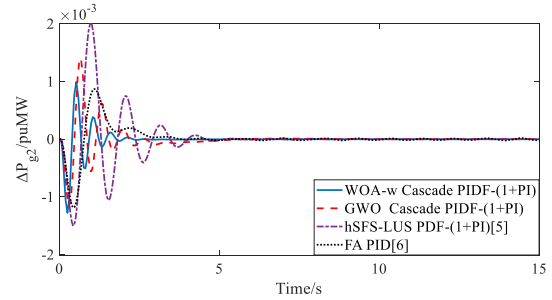

(e) ΔP_{g2}

FIGURE 11. Responses of two-area multi-unit multi-source hydro-thermal power system for $\Delta P_{D1} = 0.01$puMW.

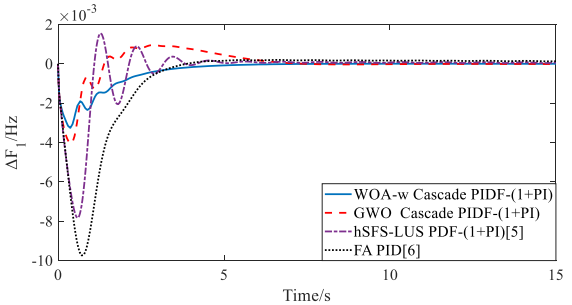

(a) ΔF_1

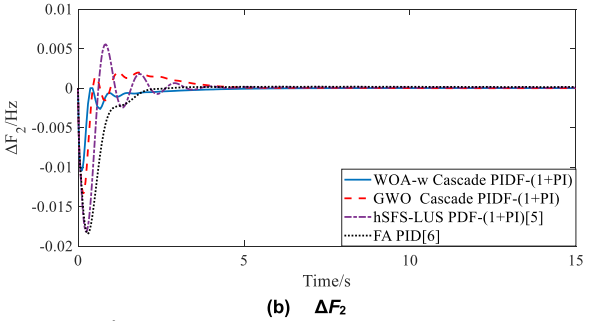

(b) ΔF_2

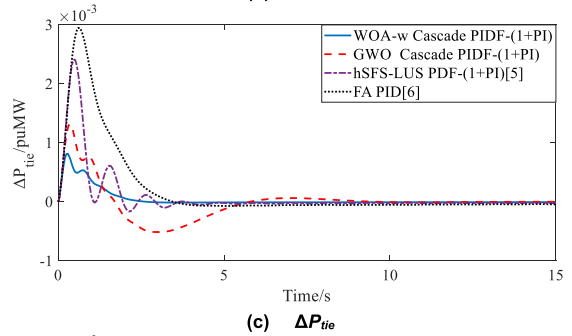

(c) ΔP_{tie}

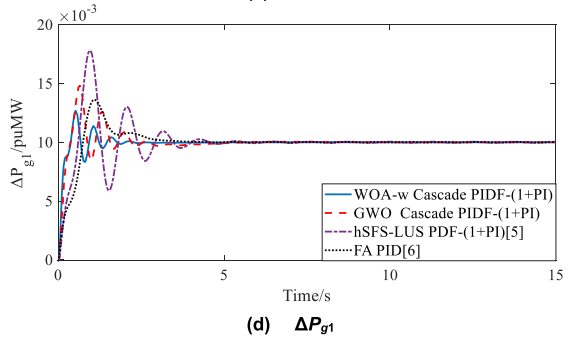

(d) ΔP_{g1}

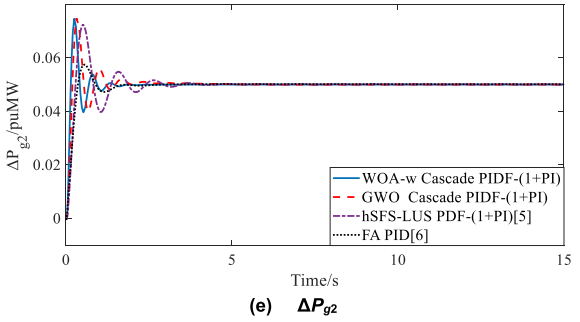

(e) ΔP_{g2}

FIGURE 12. Responses of two-area multi-unit multi-source hydro-thermal power system for $\Delta P_{D1} = 0.01$puMW and $\Delta P_{D2} = 0.05$puMW.

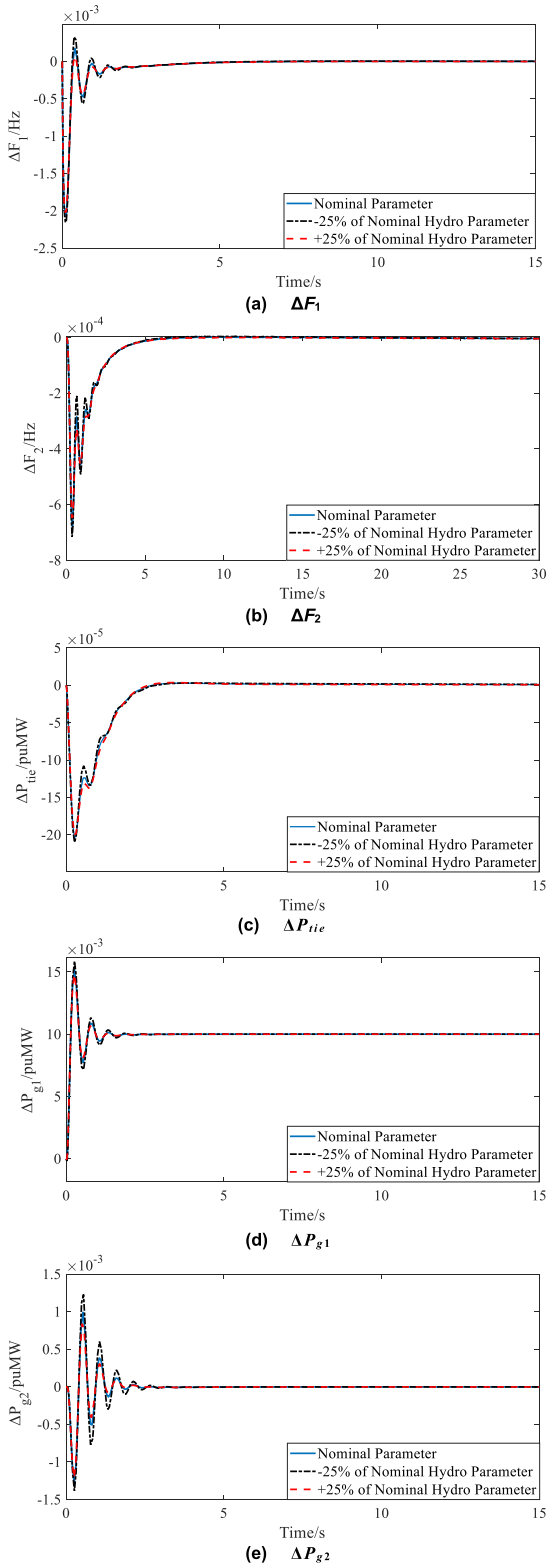

FIGURE 13. The system responses at nominal and changed parameter conditions for $\Delta P_{D1} = 0.01$puMW.

changed. It can be seen from Fig.13 and Table 7 that the system ITAE, settling time, maximum frequency deviation in each area, and maximum power deviation in the tie-line do not

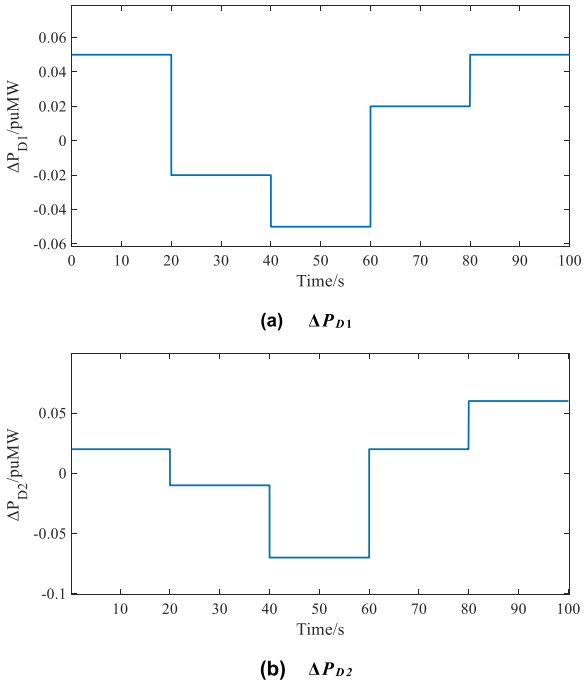

FIGURE 14. Random SLP in area-1 and area-2.

change much when the hydro unit parameters are changed. For the five settling time indicators, the largest change is for St_{F1} in the -25% of Nominal Hydro Parameter condition, which increases by 0.477s compared to the nominal condition. For the -25% of Nominal Hydro Parameter condition, the ITAE, maximum frequency deviation in area-1, maximum frequency deviation in area-2, and maximum power deviation in the tie-line vary by 13.04%, 0%, 5.88% and 5% respectively compared to the nominal condition. For the $+25\%$ of Nominal Hydro Parameter condition, the ITAE, maximum frequency deviation in area-1, maximum frequency deviation in area-2, and maximum power deviation in the tie-line vary by 4.35%, 4.76%, 4.41% and 0% respectively compared to the nominal condition. These changes are within reasonable limits. Therefore, the proposed WOA-w optimized PIDF-(1+PI) cascade controller has strong robustness and can resist the influence of system parameter changes on the dynamic performance.

B. RANDOM SLP

The load perturbations that occur in real interconnected power system are often random. The controller designed under nominal conditions must be robust enough to resist the random SLP in a real interconnected power system. It is assumed that five random load step perturbations have occurred in area-1 and area-2, as shown in Fig. 14. And the system responses with the proposed control strategy in this case are shown in Fig.15, and the settling times are shown in Table 8. Compared with the three control strategies of GWO optimized PIDF-(1+PI) cascade controller, hSFS-LUS optimized PDF-(1+PI), and FA optimized PID, the proposed

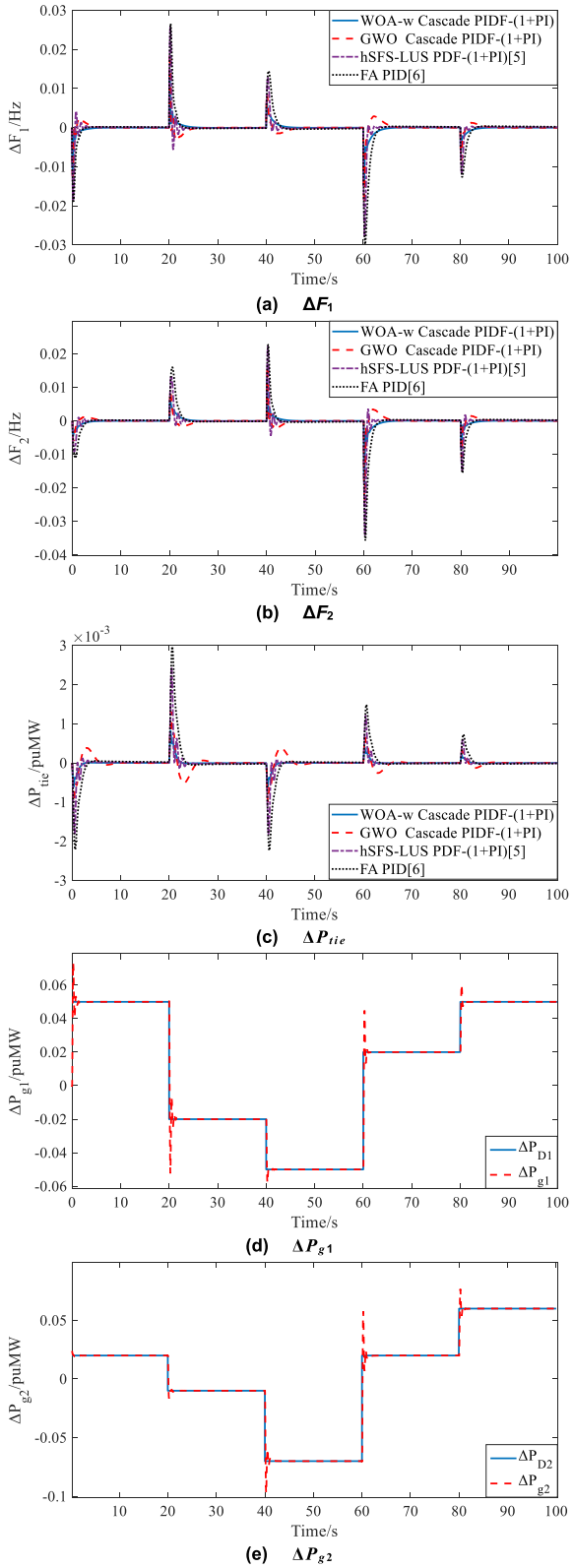

FIGURE 15. Responses of two-area multi-unit multi-source hydro-thermal power system for random SLP in area-1 and area-2.

WOA-w optimized PIDF-(1+PI) cascade controller designed with nominal conditions has shorter settling times and smaller deviations. In the whole settling period, the St_{F1} shows a

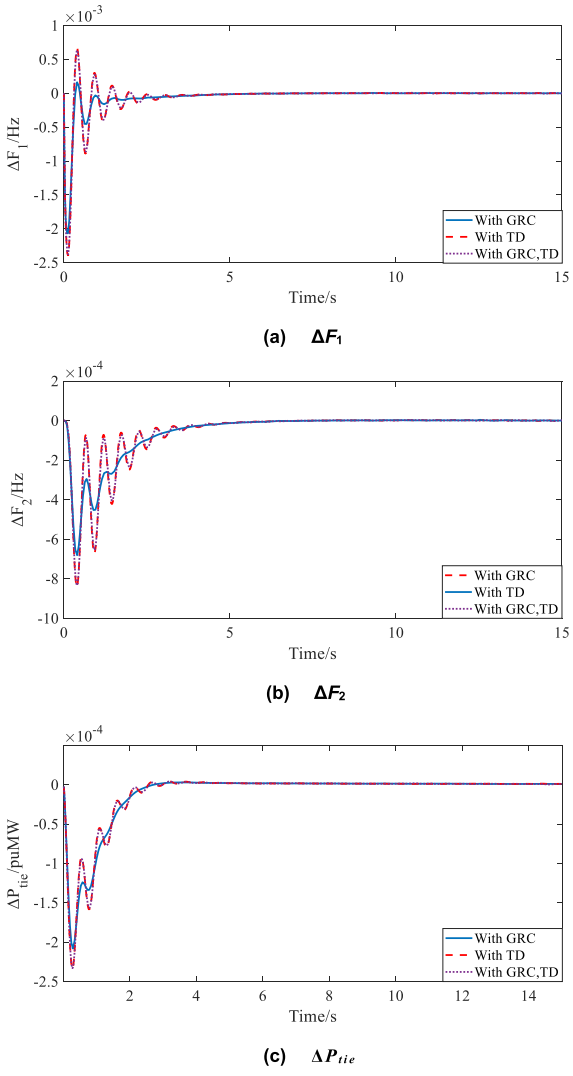

FIGURE 16. The system responses with GRC/TD/GRC&TD.

minimum reduction of 10.72% and a maximum reduction of 75.10% compared to the first two comparison control strategies, the St_{F2} shows a minimum reduction of 16.60% and a maximum reduction of 74.58% compared to the first two comparison control strategies, and the St_{Ptie} shows a minimum reduction of 22.38% and a maximum reduction of 67.24% compared to the other three comparison control strategies.

Therefore, it can be seen that the proposed control strategy has strong robustness against the effects of random SLP on the system's dynamic performance. Specifically, for the GA optimized PID controller, ΔF_1 and ΔF_2fail to stabilize within the tolerance range within 15s, but within [−0.001,0.001].

C. EFFECT OF NONLINEARITIES

In real engineering applications, nonlinearity effects must be considered, such as the generation rate constraint (GRC) of the turbine, and the time delay (TD) of the communication channel. These nonlinearity effects are part of the real power

system. However, in simulation, when the system is affected by them, it tends to produce larger frequency deviations, tie-line power deviations, and longer settling times. If the controller is not robust enough, the system will undoubtedly lose stability during real operation. Fig.16 shows the frequency deviation as well as the tie-line power deviation of the system when there are different nonlinearity effects in the system. SLP=0.01puMW in area-1. Here, the three main cases are divided into GRC in hydro unit, TD and both GRC in hydro unit & TD. GRC has ±0.045puMW/s values [37]. For TD, 0.015s transport delay at the input of controller is employed [18]. Fig.16 clearly reveals that when these nonlinearity effects are present in the system, the proposed controller is still able to reduce the frequency deviation and the tie-line power deviation to zero in a relatively short time. This indicates that the proposed controller is extremely robust.

VII. CONCLUSION

In this paper, to enhance the robustness of power system and facilitate the optimization of controller parameters, the novel WOA-w optimized PIDF-(1+PI) cascade automatic generation controller is proposed for the multi-area multi-source hydro/thermal power system with capacitive energy storage devices. The cascade controller is more suitable for stabilizing the preset-point and resisting the perturbation. The WOA-w is obtained by improving traditional WOA with introducing nonlinear time-varying adaptive weight factor, which overcomes the disadvantages of WOA and has better characteristics for the parameter optimization of AGC controller. The comparison test with GWO and WOA shows that WOA-w maintains better exploration capability at the beginning of the algorithm iteration through nonlinear time-varying adaptive weight. It can jump out of the local optimum at the partial exploitation phase, thus obtaining faster convergence speed, higher solution accuracy, and overcoming the disadvantage of easily falling into the local optimum. The effectiveness of the proposed control strategy is verified by multi-scenario cases simulation on a two-area multi-unit multi-source hydro/thermal power system containing capacitor storage units. The results show that compared with other three existing controllers, including the FA-optimized PID controller, the hSFS-LUS-optimized PIDF-(1+PI) controller, and the GWO optimized PIDF-(1+PI) cascade controller, the proposed WOA-w-optimized PIDF-(1+PI) cascade controller has better ITAE, shorter settling time, smaller maximum deviation, higher dynamic response performance, and stronger robustness.

REFERENCES

[1] R. Choudhary, J. N. Rai, and Y. Arya, "Cascade FOPI-FOPTID controller with energy storage devices for AGC performance advancement of electric power systems," *Sustain. Energy Technol. Assessments*, vol. 53, Oct. 2022, Art. no. 102671, doi: 10.1016/j.seta.2022.102671.

[2] S. Das, S. Datta, L. C. Saikia, and S. K. Bhagat, "Effect of electric vehicles and TIDN-(1+PI) controller on LFC in hydro-thermal-archimedes wave energy-geothermal-wind generations based multiarea system," in *Proc. 4th Int. Conf. Energy, Power Environ. (ICEPE)*, Apr. 2022, pp. 1–6, doi: 10.1109/ICEPE55035.2022.9798128.

[3] S. Oladipo, Y. Sun, and Z. Wang, "Application of a new fusion of flower pollinated with pathfinder algorithm for AGC of multi-source interconnected power system," *IEEE Access*, vol. 9, pp. 94149–94168, 2021, doi: 10.1109/ACCESS.2021.3093084.

[4] X. He, X. Liu, and P. Li, "Coordinated false data injection attacks in AGC system and its countermeasure," *IEEE Access*, vol. 8, pp. 194640–194651, 2020, doi: 10.1109/ACCESS.2020.3033566.

[5] R. Sivalingam, S. Chinnamuthu, and S. S. Dash, "A hybrid stochastic fractal search and local unimodal sampling based multistage PDF plus (1+PI) controller for automatic generation control of power systems," *J. Franklin Inst.*, vol. 354, no. 12, pp. 4762–4783, Aug. 2017, doi: 10.1016/j.jfranklin.2017.05.038.

[6] L. C. Saikia and S. K. Sahu, "Automatic generation control of a combined cycle gas turbine plant with classical controllers using firefly algorithm," *Int. J. Electr. Power Energy Syst.*, vol. 53, pp. 27–33, Dec. 2013, doi: 10.1016/j.ijepes.2013.04.007.

[7] D. Guha, P. K. Roy, and S. Banerjee, "Load frequency control of large scale power system using quasi-oppositional grey wolf optimization algorithm," *Eng. Sci. Technol., Int. J.*, vol. 19, no. 4, pp. 1693–1713, Dec. 2016, doi: 10.1016/j.jestch.2016.07.004.

[8] P. K. Hota and B. Mohanty, "Automatic generation control of multi source power generation under deregulated environment," *Int. J. Electr. Power Energy Syst.*, vol. 75, pp. 205–214, Feb. 2016, doi: 10.1016/j.ijepes.2015.09.003.

[9] Y. Arya, "ICA assisted FTI$^{\lambda}$DN controller for AGC performance enrichment of interconnected reheat thermal power systems," *J. Ambient Intell. Humanized Comput.*, vol. 14, pp. 1919–1935, Aug. 2023, doi: 10.1007/s12652-021-03403-6.

[10] N. Hakimuddin, I. Nasiruddin, T. S. Bhatti, and Y. Arya, "Optimal automatic generation control with hydro, thermal, gas, and wind power plants in 2-area interconnected power system," *Electr. Power Compon. Syst.*, vol. 48, nos. 6–7, pp. 558–571, Apr. 2020, doi: 10.1080/15325008.2020.1793829.

[11] Y. Arya, "Automatic generation control of two-area electrical power systems via optimal fuzzy classical controller," *J. Franklin Inst.*, vol. 355, no. 5, pp. 2662–2688, Mar. 2018, doi: 10.1016/j.jfranklin.2018.02.004.

[12] Y. Arya, "AGC of PV-thermal and hydro-thermal power systems using CES and a new multi-stage FPIDF-(1+PI) controller," *Renew. Energy*, vol. 134, pp. 796–806, Apr. 2019, doi: 10.1016/j.renene.2018.11.071.

[13] K. Peddakapu, P. Srinivasarao, M. R. Mohamed, Y. Arya, and D. J. K. Kishore, "Stabilization of frequency in multi-microgrid system using barnacle mating optimizer-based cascade controllers," *Sustain. Energy Technol. Assessments*, vol. 54, Dec. 2022, Art. no. 102823, doi: 10.1016/j.seta.2022.102823.

[14] P. Dash, L. C. Saikia, and N. Sinha, "Automatic generation control of multi area thermal system using bat algorithm optimized PD–PID cascade controller," *Int. J. Electr. Power Energy Syst.*, vol. 68, pp. 364–372, Jun. 2015, doi: 10.1016/j.ijepes.2014.12.063.

[15] S. Padhy, S. Panda, and S. Mahapatra, "A modified GWO technique based cascade PI-PD controller for AGC of power systems in presence of plug in electric vehicles," *Eng. Sci. Technol., Int. J.*, vol. 20, no. 2, pp. 427–442, Apr. 2017, doi: 10.1016/j.jestch.2017.03.004.

[16] A. Behera, T. K. Panigrahi, P. K. Ray, and A. K. Sahoo, "A novel cascaded PID controller for automatic generation control analysis with renewable sources," *IEEE/CAA J. Autom. Sinica*, vol. 6, no. 6, pp. 1438–1451, Nov. 2019, doi: 10.1109/JAS.2019.1911666.

[17] A. Behera, T. K. Panigrahi, S. S. Pati, S. Ghatak, S. Ramasubbareddy, and A. H. Gandomi, "A hybrid evolutionary algorithm for stability analysis of 2-area multi-non-conventional system with communication delay and energy storage," *Int. J. Electr. Power Energy Syst.*, vol. 130, Sep. 2021, Art. no. 106823, doi: 10.1016/j.ijepes.2021.106823.

[18] Y. Arya, "A novel CFFOPI-FOPID controller for AGC performance enhancement of single and multi-area electric power systems," *ISA Trans.*, vol. 100, pp. 126–135, May 2020, doi: 10.1016/j.isatra.2019.11.025.

[19] A. H. Yakout, M. A. Attia, and H. Kotb, "Marine predator algorithm based cascaded PIDA load frequency controller for electric power systems with wave energy conversion systems," *Alexandria Eng. J.*, vol. 60, no. 4, pp. 4213–4222, Aug. 2021, doi: 10.1016/j.aej.2021.03.011.

[20] E. Çelik, N. Öztürk, Y. Arya, and C. Ocak, "(1+PD)-PID cascade controller design for performance betterment of load frequency control in diverse electric power systems," *Neural Comput. Appl.*, vol. 33, no. 22, pp. 15433–15456, Nov. 2021, doi: 10.1007/s00521-021-06168-3.

[21] D. Guha, P. K. Roy, and S. Banerjee, "Performance evolution of different controllers for frequency regulation of a hybrid energy power system employing chaotic crow search algorithm," *ISA Trans.*, vol. 120, pp. 128–146, Jan. 2022, doi: 10.1016/j.isatra.2021.03.017.
[22] R. Loka, A. M. Parimi, S. T. P. Srinivas, and N. M. Kumar, "Region of convergence by parameter sensitivity constrained genetic algorithm-based optimization for coordinated load frequency control in multi-source distributed hybrid power system," *Sustain. Energy Technol. Assessments*, vol. 54, Dec. 2022, Art. no. 102887, doi: 10.1016/j.seta.2022.102887.
[23] T. Nie, X. He, Y. X. Yang, Q. Xiao Zhao, and Z. Z. Ning, "An improved optimization algorithm based on leapfrog and whale optimization fusion," in *Proc. 3rd Int. Conf. Natural Lang. Process. (ICNLP)*, Mar. 2021, pp. 46–51, doi: 10.1109/ICNLP52887.2021.00014.
[24] A. A. Abou El-Ela, R. A. El-Sehiemy, A. M. Shaheen, and A. E.-G. Diab, "Design of cascaded controller based on coyote optimizer for load frequency control in multi-area power systems with renewable sources," *Control Eng. Pract.*, vol. 121, Apr. 2022, Art. no. 105058, doi: 10.1016/j.conengprac.2021.105058.
[25] S. Chakraborty, S. Sharma, A. K. Saha, and S. Chakraborty, "SHADE–WOA: A metaheuristic algorithm for global optimization," *Appl. Soft Comput.*, vol. 113, Dec. 2021, Art. no. 107866, doi: 10.1016/j.asoc.2021.107866.
[26] S. Jinlong, F. Ping, and Z. Wenbin, "Lifetime improvement of digital microfluidic biochips based on the IWOA," *Microelectron. Rel.*, vol. 123, Aug. 2021, Art. no. 114182, doi: 10.1016/j.microrel.2021.114182.
[27] S. Mirjalili and A. Lewis, "The whale optimization algorithm," *Adv. Eng. Softw.*, vol. 95, pp. 51–67, May 2016, doi: 10.1016/j.advengsoft.2016.01.008.
[28] S. Dhundhara and Y. P. Verma, "Capacitive energy storage with optimized controller for frequency regulation in realistic multisource deregulated power system," *Energy*, vol. 147, pp. 1108–1128, Mar. 2018, doi: 10.1016/j.energy.2018.01.076.
[29] R. J. Abraham, D. Das, and A. Patra, "Effect of capacitive energy storage on automatic generation control," in *Proc. Int. Power Eng. Conf.*, vol. 2, 2005, pp. 1070–1074, doi: 10.1109/IPEC.2005.207066.
[30] I. Egido, L. Sigrist, E. Lobato, and L. Rouco, "Energy storage systems for frequency stability enhancement in small-isolated power systems," in *Proc. Int. Conf. Renew. Energies Power Qual.*, 2015, pp. 820–825, doi: 10.24084/repqj13.002.
[31] C. Fahrni, A. Rufer, F. Bordry, and J. Burnet, "A novel 60 MW pulsed power system based on capacitive energy storage for particle accelerators," in *Proc. Eur. Conf. Power Electron. Appl.*, 2007, pp. 1–10, doi: 10.1109/EPE.2007.4417398.
[32] K. R. M. V. Chandrakala, S. Balamurugan, and K. Sankaranarayanan, "Variable structure fuzzy gain scheduling based load frequency controller for multi source multi area hydro thermal system," *Int. J. Elect. Power Energy Syst.*, vol. 53, pp. 375–381, Dec. 2013, doi: 10.1016/j.ijepes.2013.05.009.
[33] P. C. Nayak, S. Rath, and R. C. Prusty, "Performance analysis of different FACTS devices using grey wolf optimization algorithm PDF plus (1+PI) controller based multi-area AGC system," in *Proc. Int. Conf. Renew. Energy Integr. Smart Grids, A Multidisciplinary Approach Technol. Model. Simul. (ICREISG)*, Feb. 2020, pp. 143–148, doi: 10.1109/ICREISG49226.2020.9174549.
[34] Y. Li, T. Han, H. Zhao, and H. Gao, "An adaptive whale optimization algorithm using Gaussian distribution strategies and its application in heterogeneous UCAVs task allocation," *IEEE Access*, vol. 7, pp. 110138–110158, 2019, doi: 10.1109/ACCESS.2019.2933661.
[35] D. Mishra, S. Mohapatra, P. C. Sahu, R. C. Prusty, and K. K. Baral, "Combined AGC and ELD analysis of a multi area power system with WCA based PID controller," in *Proc. Int. Conf. Adv. Power, Signal, Inf. Technol. (APSIT)*, Oct. 2021, pp. 1–6, doi: 10.1109/APSIT52773.2021.9641390.
[36] R. K. Sahu, S. Panda, and S. Padhan, "A hybrid firefly algorithm and pattern search technique for automatic generation control of multi area power systems," *Int. J. Elect. Power Energy Syst.*, vol. 64, pp. 9–23, Jan. 2015, doi: 10.1016/j.ijepes.2014.07.013.
[37] K. Zare, M. T. Hagh, and J. Morsali, "Effective oscillation damping of an interconnected multi-source power system with automatic generation control and TCSC," *Int. J. Electr. Power Energy Syst.*, vol. 65, pp. 220–230, Feb. 2015, doi: 10.1016/j.ijepes.2014.10.009.

JINGFENG MAO received the B.Eng. degree in industrial automation from the School of Automation, Wuhan University of Technology, Wuhan, China, in 1998, and the M.Sc. and Ph.D. degrees in electrical engineering from the School of Electrical and Information Engineering, Jiangsu University, Zhenjiang, China, in 2004 and 2008, respectively.

Since 1998, he has been with Nantong University, Nantong, China, where he is currently a Professor with the School of Electrical Engineering. His current research interests include electrical machines and drives, renewable energy generations and applications, and control of microgrids.

RUNDA LIU received the B.Eng. degree in electrical engineering and intelligent control from the School of Electrical Engineering, Nantong University, Nantong, China, in 2020, where he is currently pursuing the M.Sc. degree. His current research interests include renewable energy generations and automatic generation control.

AIHUA WU received the B.Eng. degree in industrial automation from the School of Electrical Engineering, Nantong University, Nantong, China, in 2000, the M.Sc. degree in electrical engineering from the School of Automation, Nanjing University of Aeronautics and Astronautics, Nanjing, China, in 2006, and the Ph.D. degree in the electrical engineering from the School of Electrical and Information Engineering, Jiangsu University, Zhenjiang, China, in 2019.

Since 2000, she has been with Nantong University, where she is currently an Associate Professor with the School of Mechanical Engineering. Her current research interests include electrical machines and drives and renewable energy generations and applications.

SHANG WU received the B.Eng. degree in water conservancy and hydropower engineering from the School of Water Conservancy and Environmental Engineering, Zhejiang University of Water Resources and Electric Power, Hangzhou, China, in 1999. He is currently an Engineer with Nantong Offshore Construction and Engineering Company Ltd. His current research interests include offshore wind power generation and battery energy storage systems.

JIANJUN HE received the B.Eng. degree in industrial automation from the School of Automation, Wuhan University of Technology, Wuhan, China, in 1996. He is currently a Senior Engineer with Nantong Offshore Construction and Engineering Company Ltd. His current research interests include offshore wind power generation and distribution network control.